An Aniline-Complexed Bismuth Tungstate Nanocomposite Anchored on Carbon Black as an Electrode Material for Supercapacitor Applications

Sheoran, Karamveer; Devi, Nishu; Alsanie, Walaa F.; Siwal, Samarjeet Singh; Thakur, Vijay Kumar

Published in:
ChemistrySelect

DOI:
10.1002/slct.202301878

Print publication: 13/11/2023

Document Version
Publisher's PDF, also known as Version of record

ChemistrySelect

Research Article
doi.org/10.1002/slct.202301878

Chemistry Europe
European Chemical Societies Publishing

www.chemistryselect.org

An Aniline-Complexed Bismuth Tungstate Nanocomposite Anchored on Carbon Black as an Electrode Material for Supercapacitor Applications

Karamveer Sheoran,[a] Nishu Devi,[b] Walaa F. Alsanie,[c] Samarjeet Singh Siwal,*[a, d, e] and Vijay Kumar Thakur*[e, f]

The development of efficient electrode materials for supercapacitors has been a topic of extensive research. In this study, a novel electrode material composed of carbon black anchored bismuth-tungstate-aniline complex ($Bi_2(WO_4)_3$/Aniline/CB) (BTACB) nanocomposite was synthesized for supercapacitor applications. The BTACB nanocomposite exhibited excellent electrochemical properties with a specific capacitance of 306 F/g at a current density of 1 A/g and excellent cycling stability. The improved electrochemical performance of the BTACB electrode material is attributed to the synergistic effects of the bismuth-tungstate and aniline complex, and the conductive carbon black, which provides high surface area and good conductivity. These findings suggest that the carbon black anchored bismuth-tungstate-aniline complexed electrode material is a promising candidate for high-performance supercapacitors.

Introduction

The rapid modernization and industrialization have shown a tremendous surge in energy needs over the previous years. The major supply of the community's electricity demands is mainly based on petroleum-based fuels. There is an apparent necessity for other energy sources within the restricted petroleum resources.[1] Consequently, there has been a continuous need of renewable energy resources and to store that energy developing interest in high-power and competent energy-density storage techniques and procedures is visible throughout the research field. With the environmental contamination induced by the explosion of fossil fuels, numerous investigators are intent on designing novel energy storage tools[2] An illustration of such an appliance is a supercapacitor (SC), also comprehended as an electrochemical double-layer capacitor (EDLC) or an ultra-capacitor.[3] SC as an energy storage device has the benefits of increased power density (PD), high coulomb efficiency, long-lasting life, broad temperature range, and good protection, and is one of the most encouraging nominees towards power storage approaches.[4] It can recreate a vital role in energy storage and become a unique energy storage appliance to help the global energy problem and satisfy the rising human consumption market.

Based on the charge storage mechanism, SCs are generally split within EDLCs, Pseudocapacitors, and hybrid SCs.[5] Different aspects define the electrochemical activity of SCs, for example, the electrode material's character, the electrolyte's arrangement, and the typical working conditions.[6] The electrode substances are primarily split within the carbon, metal oxides, conductive polymers (CP), etc..[7] With the added consequence of materials science in current years, novel materials like MOF and MXene have acquired much concentration.[8]

Many nanomaterials with high electrochemical capacitance performance have been used broadly as electrode materials in SCs because they can improve charge assembly and ion transport, particularly for carbon materials, CPs, and transition-metal oxides/hydroxides. Regrettably, the inadequate electronic/ionic conductivity of single metal oxides/hydroxides and the quickly demolished polymer backbone of CPs significantly restrict the rate and cycling arrangements.[9] Further, Chen et al.[10] reported CP-based materials (such as poly(aniline-*co*-azure B), Reduced Graphene Oxide/Poly(*N*-methylthionine) and Poly(azure C)-coated CoFe Prussian blue) for SCs applications. Mtz-Enriquez et al.[11] reported the electrochemical properties of graphene SCs that use flexible graphene electrodes (FGEs)

[a] *Dr. K. Sheoran, Dr. S. S. Siwal*
Department of Chemistry, M.M. Engineering College, Maharishi Markandeshwar (Deemed to be University), Mullana-Ambala, Haryana, 133207, India

[b] *Dr. N. Devi*
Mechanics and Energy Laboratory, Department of Civil and Environmental Engineering, Northwestern University, 2145 Sheridan Road, Evanston, IL60208, USA

[c] *Dr. W. F. Alsanie*
Department of Clinical Laboratories Sciences, The Faculty of Applied Medical Sciences,
Taif University, P.O. Box 11099, Taif 21944, Saudi Arabia

[d] *Dr. S. S. Siwal*
Department of Chemical Engineering Technology, University of Johannesburg, P.O. Box 17011, Doornfontein, 2088, South Africa

[e] *Dr. S. S. Siwal, Prof. V. K. Thakur*
Biorefining and Advanced Materials Research Center, SRUC, Kings Buildings, Edinburgh, EH9 3JG, UK
E-mail: Vijay.Thakur@sruc.ac.uk
Samarjeet.Siwal@sruc.ac.uk

[f] *Prof. V. K. Thakur*
School of Engineering, University of Petroleum & Energy Studies (UPES), Dehradun, Uttarakhand, India

covered with V_2O_5 (VO_x) or carbon nanotubes (CNTs)/VO_x films. Additionally, carbon-based materials have been used for the SCs applications by different researchers.[12]

Bismuth tungstate (BiW) and their nanocomposite-based materials have been broadly utilized for catalytic applications owing to their economic, improved electron transfer kinetics, quick reaction, easy availability, and superior resilience.[13] Scientists tried different kinds of preparation methods to design highly functional BiW and their nanocomposites, like sol-gel,[14] chemical vapor deposition,[15] the co-precipitation process,[16] and the hydrothermal process.[17] Nevertheless, the BiW nanocomposite regularly exhibited low catalytic behaviour owing to its semi-conducting character (band gap ~2.8 eV),[18] low electrical conductivity, inadequate electron transfer kinetics, and a minimal numeral of active sites.

The presence of CB and aniline complexation enhances the surface area of the BiW-nanocomposite electrode.[19] The combination of BiW and CB, along with the aniline complexation, results in a synergistic effect that enhances the electrochemical performance of the SC electrode. This leads to increased specific capacitance and improved energy density, making the electrode more efficient in storing and delivering electrical energy. Therefore, the BTACB nanocomposite electrode material offers high performance, stability, cost-effectiveness, and environmental friendliness, making it a promising choice for SC applications over traditional electrode materials. Table 1 shows the electrochemical parameters of Bismuth-based materials as a SC application.

This work presents a novel synthesis method of Bismuth tungstate nanoparticles supported with aniline matrix and anchored with carbon black. This electrode assembly shows improved electrochemical performance of the BTACB nanocomposite which is attributed to the synergistic effects of the bismuth-tungstate and aniline complex, and the conductive carbon black, which provides high surface area and good conductivity. This paper is divided into two fractions: the first provides information related to the material's characterization, and the second elucidates the electrochemical activity of the synthesized material towards SCs application.

Materials and methods

Chemicals and reagents

All reagents and chemicals such as aniline, bismuth nitrate penta hydrate (Bi $(NO_3)_3 \cdot 5H_2O$), nitric acid (HNO_3), sodium tungstate (Na_2WO_4), polyvinylidene difluoride (PVDF), ethyl acetate (EA), methanol, and ethanol were obtained from Merck (St. Louis, MO, USA) and utilized without further purification. Millipore ultrapure deionized water (dH_2O) was used wherever required.

Preparation of $Bi_2(WO_4)_3$/Aniline/CB (BTACB) nanocomposite

Bismuth tungstate (Bi_2WO_6) was synthesized by using a wet chemical approach. In a typical synthesis method as shown in Figure 1(a) bismuth nitrate ($Bi(NO_3)_3$) with a concentration of 0.1 mol dm^{-3} was prepared by dissolving the bismuth salt in nitric acid and adding deionized water. Freshly prepared bismuth nitrate solution was added dropwise to the methanolic solution of aniline (1.0 mol dm^{-3}) at room temperature with the immediate formation of a white colour precipitate forming a bismuth aniline inorganic-organic complex.[9f] Further, an aqueous solution of sodium tungstate (0.3 mol dm^{-3}) was added to the white precipitate. The Bi^{+3}/aniline complex formed in the previous step combined with the tungstate ions from sodium tungstate solution resulted in formation of Bismuth tungstate nanoparticles complexed with aniline (BTA). The reaction mixture was left under stirring conditions for 6 h at room temperature.

The solid material formed as BTA was centrifuged and kept for drying at 80 °C for 24 h. The dried material was subjected to optical, microscopic, and structural characterization. The electrochemical impedance spectroscopy (EIS) technique has been used to demonstrate the synthesized material's internal resistance and charge transfer properties. The synthesized material was doped with 10 wt% of carbon black to find out the charge storage ability of the system for electrochemical supercapacitor application. The final nanocomposite was tested as a supercapacitor electrode material and represented as BTACB nanocomposite throughout the manuscript.

Table 1. Electrochemical performance of bismuth-based materials in SC application.

Bi-based materials	Electrolyte solution	Specific capacitance	Current density	Energy density	Ref.
Ultrathin Bi_2O_3 nanowires	6 M KOH	691.3 F/g	2 A/g	138.3 Whkg^{-1}	[20]
Bi_2O_3/Ni foam/graphite/Asymmetric SC	6 M KOH	37 F/g	1 mA/cm^2	11 Whkg^{-1}	[21]
MIL 53(Al)/Bi_2WO_6	3 M KOH	220 F/g	0.5 A/g		[22]
Graphene/Bi_2O_3	–	136.76 F/g	0.5 A/g	–	[23]
Bi_2S_3//Ni foam//AC Hybrid SC	1 M KOH	148.7 F/g	1 A/g	45.1 Wh/kg	[24]
Bi_2S_3	1 M Na_2SO_4	185.7 F/cm^2	1 mA/cm^2	–	[25]
rGO/Bi_2O_3	6 M KOH	94 F/g	0.2 A/g		[26]
BTACB	1 M KOH	306 F/g	1 A/g		Current study

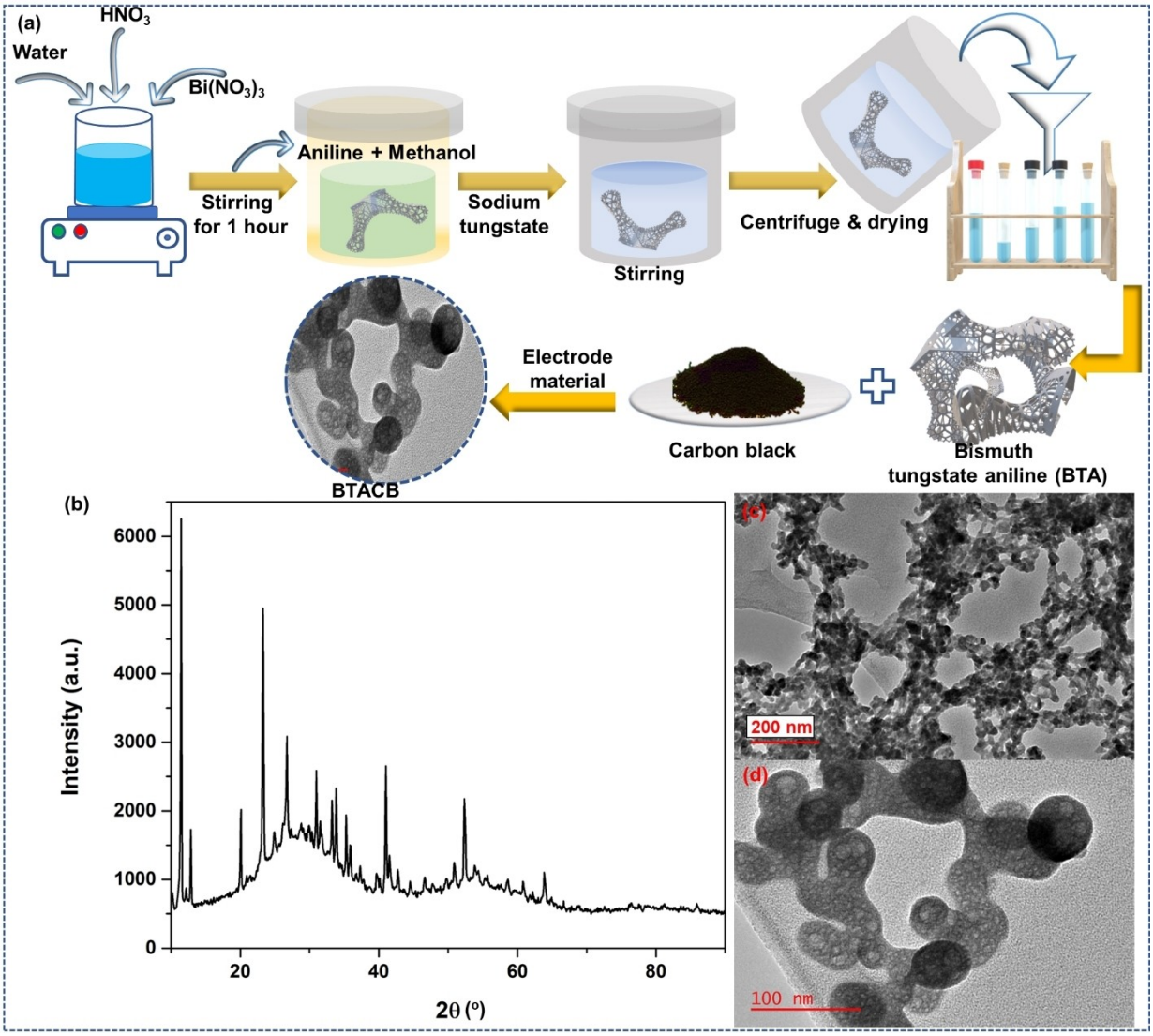

Figure 1. **(a)** Synthesis process of BTA nanocomposite. **(b)** XRD pattern of BTA. TEM images of **(c)** bismuth-aniline complex and **(d)** BTA nanocomposite.

Modification of GCE electrode

Three electrode systems consisted of a glassy carbon electrode of 3 mm in diameter as the working electrode (WE), Hg/HgO as the reference electrode and Pt wire as the counter electrode. The BTACB was finely grounded using a mortar pestle and well mixed with polyvinylidene difluoride (PVDF) as binder and ethyl acetate (EA) as a solvent to prepare a slurry in 80:10:10 weight ratio. The WE were modified with the BTACB/PVDF/EA slurry by drop and dry technique. The surface of the glassy carbon electrode was scrubbed and cleaned before each application. The surface was rinsed by using alumina solutions with different concentrations and ultrasonication. To confirm the cleaned surface of WE, etching of aqua regia was utilized, and after the cleaning process, further electrochemical analysis was performed by incorporating the material on WE. All the studies based on electrochemistry were performed in a covered cell.

Electrochemical analysis

Electrochemical workstation (Bio-Logic SP 200) was used for the electrochemical analysis, which is connected to data controller. Here, in the electrochemical system, we used a three-electrode method: a glassy carbon electrode (GCE), saturated calomel and platinum electrode were used as a working, reference, and the counter electrode, respectively, to characterize the electrochemical characteristics of the synthesized material. In this process, an alkaline media of KOH (1 mol dm^{-3}) was utilized as the electrolyte. This study applied a drop-and-dry method to incorporate the prepared material (on GCE) on the working electrode. Cyclic voltammetry (CV) within potential range of −1.0 to 0 V at scan rate of 5 to 200 mV/s and galvanostatic charge-discharge (GCD) within potential window of −1.0 to 0 V at current density of 10 to 1 A/g were conducted for the confirmation of suitability of the synthesized materials towards energy storage in SCs. The impedance property of nano-

composite was estimated utilizing Biologic SP-200 fitted with electrochemical impedance spectroscopy (EIS) within the frequency spectrum from 200 kHz to 1 Hz at open circuit potential in multisine mode at a voltage amplitude of 10 mV.

Material characterization

Utilized different microscopic and spectroscopic techniques to illustrate the synthesized nanocomposite. Fourier transform infrared (FTIR) spectroscopy was employed to ensure the accurateness of functional groups of the synthesized nanocomposite material by linking the related FTIR peaks of the synthesized nanocomposite. Here, an FTIR spectrometer (IRSpirit QATR-S; A224057 00293-Shimadzu, Kyoto, Japan) was utilized for investigation. XRD was performed on a Rigaku X-ray diffractometer (MinifexII Desktop) with Cu $K\alpha$ radiation (Rigaku Corporation, Tokyo, Japan). The microscopic effects of the prepared nanocomposite were performed at 200 kV applying Tecnai G2 TF30 (JEOL, Tokyo, Japan) transmission electron microscope (TEM). The composite substance's surface area and pore size spreading of the samples were evaluated by N_2 adsorption-desorption relying on the Brauner-Emmet-Teller (BET) plus Barrett-Joyner-Halenda (BJH) (Quantachrome Instrument, Boynton Beach, FL, USA) technique (Belsorp-BELMAX).

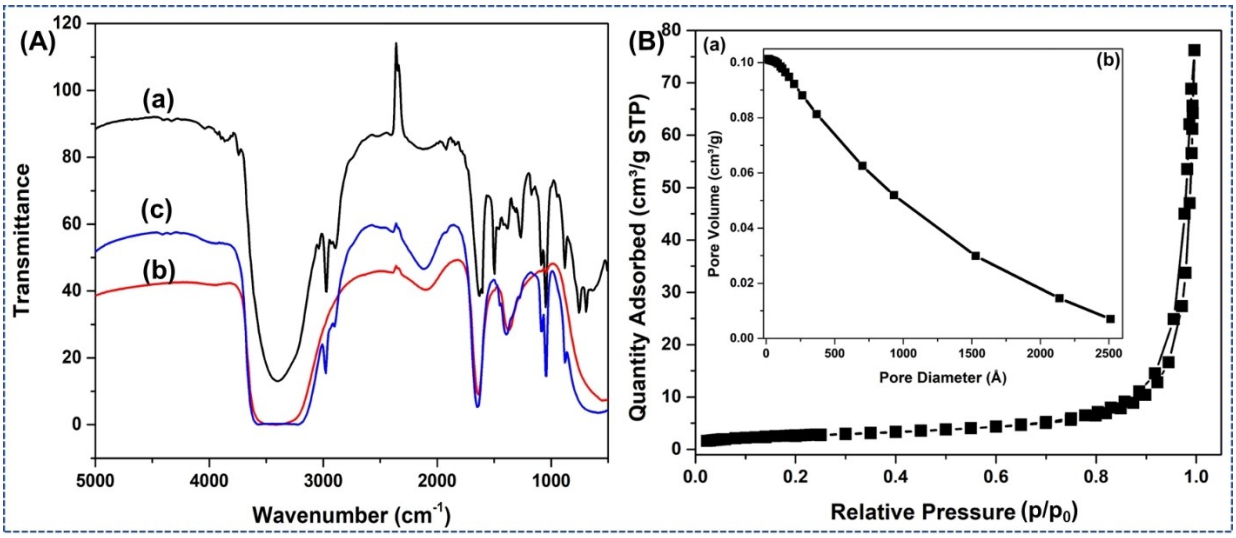

Figure 2. **(A)** FT-IR spectra investing the functional groups and characteristic vibrations within the three materials. **(a)** aniline **(b)** bismuth-aniline complex, and **(c)** bismuth-tungstate-aniline complex. **(B)** **(a)** N_2 adsorption-desorption isotherms of the bismuth-tungstate-aniline complex; **(b)** BJH pore-size diffusion curve of the bismuth-tungstate-aniline complex.

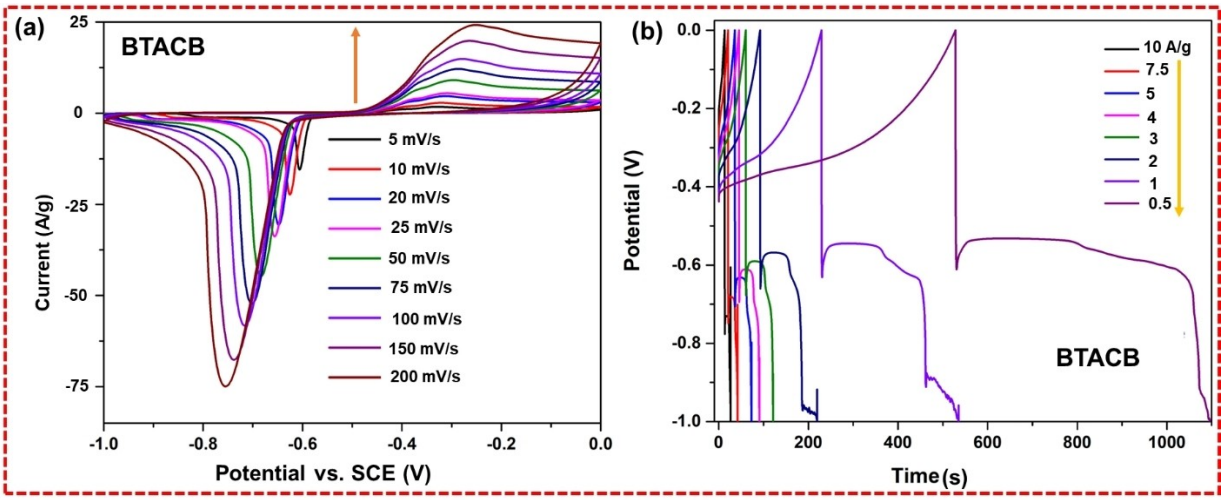

Figure 3. **(a)** CV analysis of BTACB nanocomposite at different scan rates. **(b)** GCD analysis of BTACB nanocomposite at different current density.

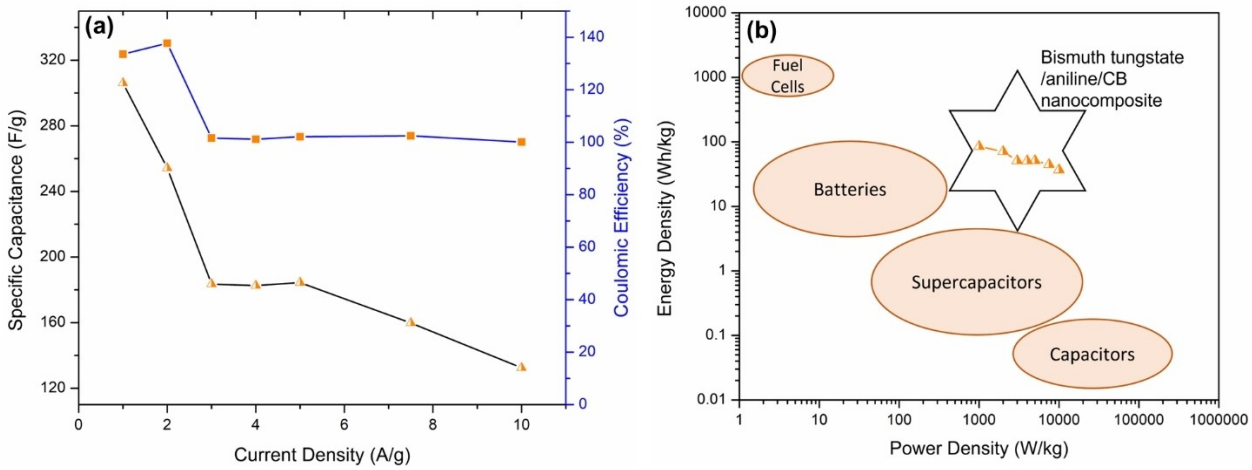

Figure 4. **(a)** Specific capacitacne and coulombic efficiency of BTACB nanocomposite at several current density **(b)** Ragone plot showing the energy and power densities of synthesized BTACB nanocomposite electrode material with respect to different energy storage devices.

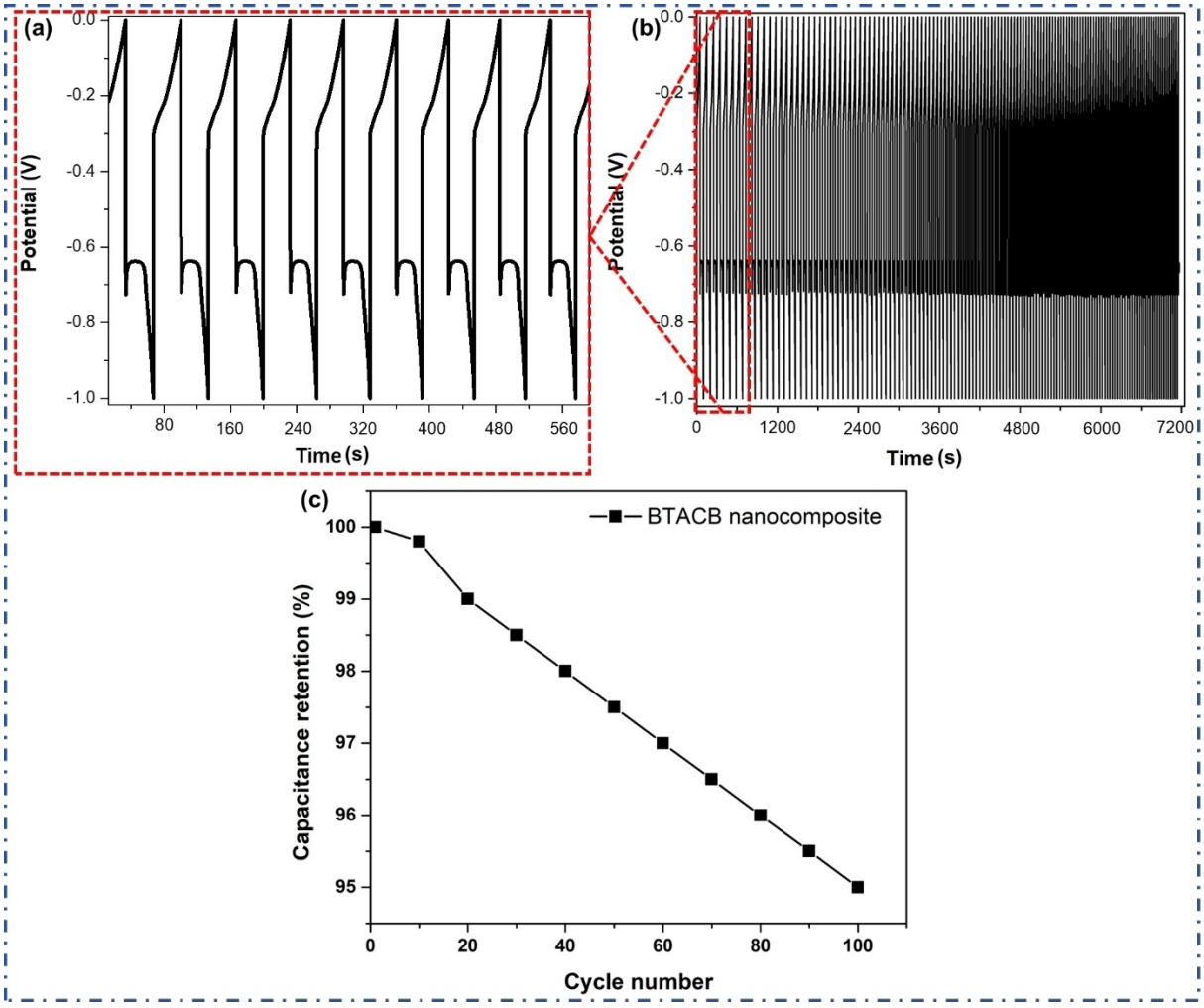

Figure 5. Shows the 100 GCD cycle life stability of BTACB nanocomposite **(b)**, GCD curve for 9 consecutive cycles at current density 5 Ag^{-1} **(a)** and **(c)** capacitance retention vs. cycle number curve of GCD of BTACB nanocomposite.

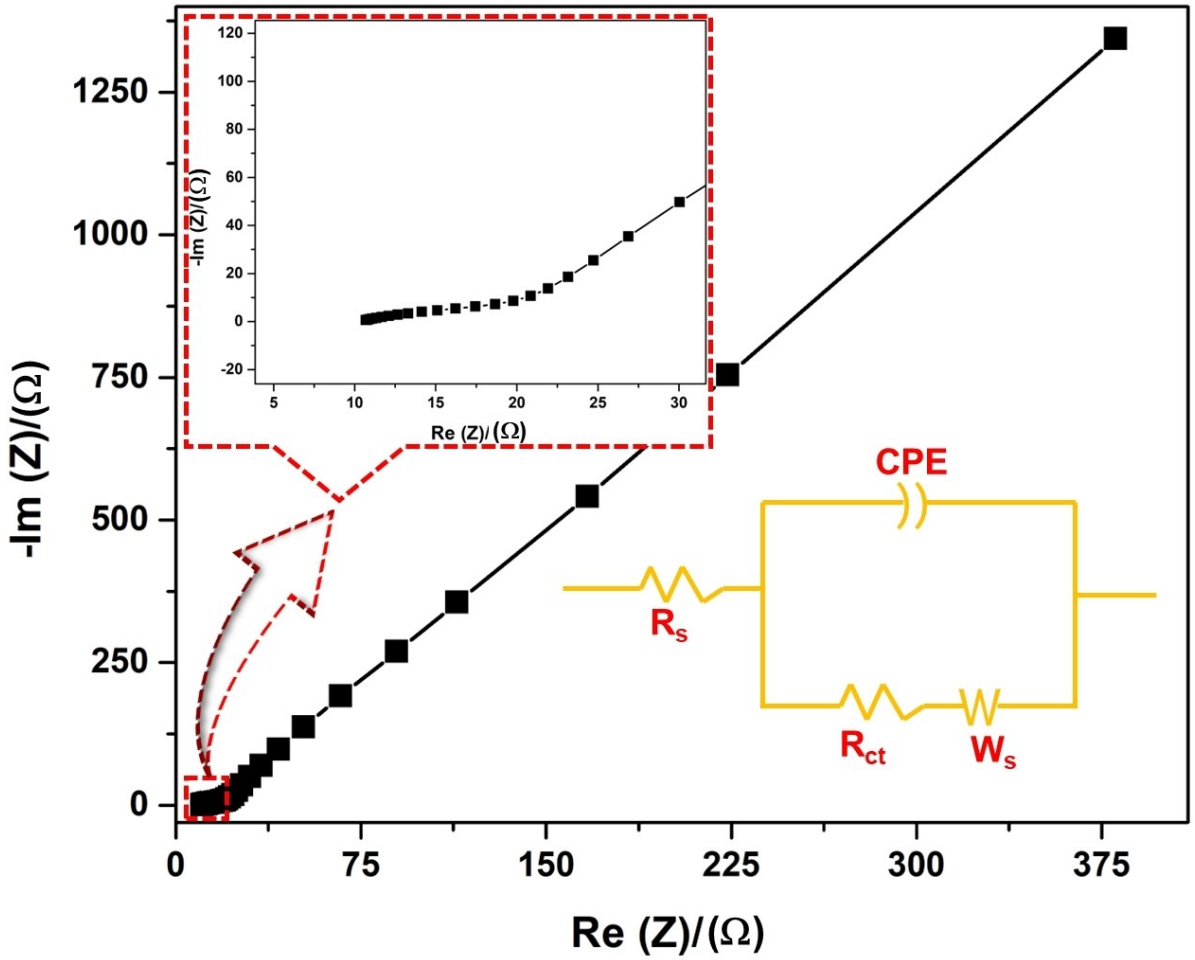

Figure 6. Electrochemical impedance spectra of BTACB, Z′ is real impedance and Z″ is imaginary impedance (inset figures shows the zoom in area of high frequency range).

Results and Discussion

Material Characterization

Structural, morphological, and optical analysis

The BTA (Bismuth Tungstate) nanoparticles, stabilized with aniline, were thoroughly characterized, and revealed significant attributes. The synthesized BTA nanoparticles were analysed using X-ray diffraction, as illustrated in Figure 1(b). The most intense peak at approx. 23° show the formation of bismuth-tungstate. The diffraction peaks in the PXRD graph are connected to the orthorhombic phase of the BTA nanoparticles, observed from 28° to 90°. This phase was also compared with the international centre diffraction data (JCPDS) card No. 73-1126 having lattice parameters a = 5.457, b = 5.436 and c = 16.42 Å. The diffraction peaks of BTA centred at 2θ degree values are 28.29, 32.79, 32.91,36.81, 47.14, 50.08, 55.75, 58.46, 75.92, 78.53, and 87.50 have planes (113), (200), (002), (200), (202), (220), (133), (040), (391), (204), and (462) respectively, which were elucidated to the typical crystal planes. The sharp and distinct peaks of the solid BTA powder revealed that the material is crystalline.[27]

The morphology of nanocomposite was observed using the transmission electron microscopic (TEM) technique. The TEM images of the nanomaterial before and after the addition of sodium tungstate are showcased in Figure 1(c, d) which clearly shows the aniline bismuth complexation chemistry and porous nature. The acquisition of tungstate shows the TEM picture of the particles, where the aniline complexation probably limited the visibility of the lattice edges. At the same time, TEM also revealed that BTA complex was within the nanometer range, and the material was crystalline. The light shadow in the TEM image showed the presence of a organic-inorganic complex chain, and the dark shadows in the image revealed the existence of trapped bismuth tungstate nanoparticles.[9d]

FT-IR spectra of aniline, bismuth-aniline complex and bismuth-tungstate-aniline nanoparticles were observed and recorded to know the optical characteristics of all three products and formation of composite as shown in Figure 2A(a–c). The bands observed at 3429 cm^{-1} are broad and shows the stretching of NH group, which shows the presence of uncondensed groups of amines. On the other hand, the presence of

nitrogen-containing groups was confirmed by the presence of two strong bands at 1653 and 1494 cm^{-1} because of different stretching vibrations of aniline.[28] The presence of the C–H group was confirmed by its bending vibration, which gives an adsorption band at 1114 and 2096 cm^{-1}. The various bands or peaks are in concurrence and obtained concerning all three prepared materials.[9c,29]

The nitrogen adsorption/desorption examinations were conducted on the solid powdered BTA nanoparticles to explore the influence of pore dimensions on the charge capacitance behaviour of the electrode nanocomposite. These tests revealed that BTA has a potential to exhibit superior capacitance behaviour, making it a promising electrode material. As demonstrated within Figure 2B(a), the calculated BET-specific surface area is 9.6245 $m^2 g^{-1}$ for aniline stabilized bismuth-tungstate nanoparticles. The isotherm shows the presence of various pore sizes from micro- to macropores. The growing adsorbed volume at low pressure corresponds to micropores; the adsorbed volume at medium comparative pressure indicates the presence of mesopores, and that at a relative pressure around 1.0 (>0.9) indication of macropores.[30] Figure 2B(b) shows the samples' Barrett-Joyner-Halenda (BJH) pore-size dispersals. According to the Brunauer-Deming-Deming-Teller (BDDT) type, the isotherms of BTA show the specific kind IV with an H_2 hysteresis loop, indicating the presence of mesoporous network, which should arise from the gap spaces among bismuth tungstate nanoparticles and aniline complex.

Electrochemical Analysis

To analyse the electrochemical performance of the prepared BTACB i.e. ($Bi_2(WO_4)_3$/Aniline/CB) nanocomposite as supercapacitor electrode material, a typical three-electrode system was utilized, as explained in the abovementioned section. Cyclic voltametric (CV) technique and galvanostatic charge-discharge (GCD) were performed to determine the redox behaviour, charge storage ability and life cycle of the nanocomposite.

Cyclic voltammetry (CV) is the initial stage that helps in the identification of EDLC or the pseudocapacitive nature of electrode materials and hence hypothesizing the charge storage mechanism. Figure 3(a) shows the CV of BTACB nanocomposite at different scan rates from 5 mV/s to 200 mV/s. The typical redox peaks present in CV curves confirmed the pseudocapacitive nature of the BTACB nanocomposite which is a combination of storage due to redox reactions and EDLC. The significant oxidation and reduction peaks in CV directed towards battery type charge storage mechanism of BTACB where charge storage due to redox reactions of bismuth ($Bi^{3+} \leftrightarrow Bi^0$)[9f] predominates. It leads to storage of charge carriers i.e., electrons and ions in its crystal lattice by reversible intercalation or deintercalation. On the other hand, the aniline complex provided the stabilization effect in the backbone with enhanced dispersion and interaction with nanoparticles. Anchoring of carbon black contributes towards charge storage via double layer formation. It provides additional active sites and excellent conductive pathway due to its higher conductivity that ultimately facilitates electron transfer required for redox reactions. Additionally, the porous structure of BTACB nanocomposite also facilitates ion diffusion and mass transport of ions. The redox peaks obtained in the forward scan shows the increase in current density. The progressively increased current density value with continuously repeated scan rates from 5 mV/s to 200 mV/s resulted in a shift in peak potential value shows the improved performance of the material by shifting the peak upward at the same potential.

The charge storage mechanism can be supported with the GCD profiles of BTACB nanocomposite. The plateau in discharge curve again represents pseudocapacitive behaviour of the material due to active sites of bismuth.[9c] GCD curves of bare and all modified electrodes within the potential window of −1.0 to 0 V with different current densities are showcased in Figure 3(b). The distorted shape of the graph demonstrated the high charge-storage capacity of aniline-bismuth-tungstate nanomaterial. The specific capacitance of the nanocomposite was measured by the following equations (1 to 4):[31]

$$C_s = (i^* \Delta t)/(m^* \Delta V) \quad (1)$$

$$ED = (i^* \Delta V^* \Delta t^* 1000)/(m^* 3600) \quad (2)$$

$$PD = (i^* \Delta V^* 1000)/m \quad (3)$$

$$\eta = \left(\frac{t_d}{t_c}\right) \times 100 \quad (4)$$

Where Cs represents the specific capacitance of the nanocomposite in F/g, ED energy density in Wh/kg, PD power density in W/kg, η coulombic efficiency in %, Δt represents the discharge time in seconds, ΔV is the potential difference in V, I is the current applied to the electrode in A and m as mass of electrode on glassy carbon electrode surface in g an therefore i/m is the current density of the system in A/g. The highest specific capacitance of the system was 306 F/g at 1 A/g.

The decline of specific capacitance during the cycling method would be due to the material's mechanical fatigue effects generated through the constant loading and unloading of the ions from the media. A reverse manner has been marked for the BTACB-doped electrode, where a growth in specific capacitance value has been received on the different current densities (Figure 4(a)). Figure 4(b) shows the Ragone plot, which is between the energy and power densities of synthesized BTACB nanocomposite electrode material with respect to different energy storage devices.

Long-term resilience is one of the aspects that is liable for the practical applications of SCs and The cyclic stability of synthesized nanocomposite material is an imperative parameter for itsapplication. The cycling stability plots as shown in Figure 5 from more than 100 repetitive charge-discharge cycles exhibited a high performance with repetitive cycles. which supported that the BTACB nanocomposite is a promising electrode material for SC incorporation wherecarbon black assisted in improving cyclic stability. It has been observed that the good cyclic strength shows 95% capacitance retention for

100 cycles. The first 9 longer CD cycles at current density 5 A/g are given in Figure 5(a). Further, Figure 5(c) shows the capacitance retention vs. cycle number curve of GCD of BTACB nanocomposite.

This slight drop might be due to the deterioration of the electrode material during constant charging and discharging in 1 M KOH electrolyte or the leaching of the material from a vertically assembled glassy carbon electrode in an electrochemical cell.

Electrochemical Impedance Spectroscopy (EIS) was performed to study further the internal resistance, charge transfer kinetics, and ion diffusion process of BTACB nanocomposite as SC electrode material. The EIS was measured in a frequency range of 200 kHz to 1 Hz. As shown in Figure 6, the intercept between the impedance spectrum and real impedance axis correspondence to equivalent series resistance (ESR) of the nanocomposite shows comparable ESR around 5 Ω. The Nyquist plot showed the negligible high-frequency resistor-capacitor loop or semicircle associated with charge transfer resistance at the electrode/solution interface.[32] In the low-frequency portion of the plot, the arcs tend toward a fixed line showing that BTACB displays nearly ideal capacitive behaviour with sound ion distribution within the electrode network. The diameter of the semicircle for the BTACB electrode around 10 Ω was the very low, which signifies the high conductivity and low inner resistance. This is due to the carbon black in BTACB nanocomposite, which is increased its surface area. The outcomes implied that BTACB exhibited the highest conductivity or lowest internal resistance, including polarization impedance.

Conclusion

In conclusion, the development of the carbon black anchored bismuth-tungstate-aniline complexed electrode material represents a significant step forward in the field of supercapacitor technology. This novel material showed excellent electrochemical properties, including a high specific capacitance and good cycling stability, making it a promising candidate for use in high-performance supercapacitors. The results suggest that the synergistic effect of the carbon black support and the bismuth-tungstate-aniline complex significantly improved the conductivity and electrochemical activity of the material.

As for prospects, there are several avenues for further research. The first would be to explore the scalability of the synthesis process for large-scale production. The second would be to investigate the mechanism of charge storage in the material, which could provide insights into how to further optimize its electrochemical performance. Additionally, the compatibility of the material with different electrolytes and its long-term stability under different operating conditions could also be studied.

In summary, the carbon black anchored bismuth-tungstate-aniline complexed electrode material developed in this study represents a promising candidate for high-performance supercapacitor applications. Further research can help to optimize and scale up the material for practical use in energy storage applications.

Acknowledgements

The authors acknowledge the support from the Department of Chemistry and Research & Development Cell of Maharishi Markandeshwar (Deemed to be University), Mullana, Ambala, Haryana, India. W.F.A. would like to acknowledge the Taif University TURSP program (TURSP-HC2023/5) for funding. SSS would like to acknowledge the financial support provided by the UKRI via Grants No EP/T024607/1. VKT would like to acknowledge the Research support provided by the the UKRI via Grant No. EP/T024607/1; and Royal Society via grant number IES\R2\222208.

Conflict of Interests

The authors declare no conflict of interest.

Data Availability Statement

The data that support the findings of this study are available from the corresponding author upon reasonable request.

Keywords: charge-discharge process · energy storage applications · metal-based nanomaterials · supercapacitors

[1] a) G. Wang, L. Zhang, J. Zhang, *Chem. Soc. Rev.* **2012**, *41*, 797–828; b) M. Armand, J. M. Tarascon, *Nature* **2008**, *451*, 652–657.
[2] J. Ding, H. Gao, K. Zhao, H. Zheng, H. Zhang, L. Han, S. Wang, S. Wu, S. Fang, F. Cheng, *J. Power Sources* **2021**, *487*, 229369.
[3] a) R. Vinodh, Y. Sasikumar, H.-J. Kim, R. Atchudan, M. Yi, *J. Ind. Eng. Chem.* **2021**, *104*, 155–171; b) P. Sharma, T. S. Bhatti, *Energy Convers. Manage.* **2010**, *51*, 2901–2912; c) Y. Zhang, H.-x. Mei, Y. Cao, X.-h. Yan, J. Yan, H.-l. Gao, H.-w. Luo, S.-w. Wang, X.-d. Jia, L. Kachalova, J. Yang, S.-c. Xue, C.-g. Zhou, L.-x. Wang, Y.-h. Gui, *Coord. Chem. Rev.* **2021**, *438*, 213910.
[4] a) A. Muzaffar, M. B. Ahamed, K. Deshmukh, J. Thirumalai, *Renewable Sustainable Energy Rev.* **2019**, *101*, 123–145; b) M. Du, Q. Li, Y. Zhao, C.-S. Liu, H. Pang, *Coord. Chem. Rev.* **2020**, *416*, 213341; c) Y. Zhang, S.-c. Xue, X.-h. Yan, H.-L. Gao, K.-z. Gao, *Electrochim. Acta* **2023**, *442*, 141822.
[5] a) E. Lim, C. Jo, J. Lee, *Nanoscale* **2016**, *8*, 7827–7833; b) N. R. Chodankar, H. D. Pham, A. K. Nanjundan, J. F. S. Fernando, K. Jayaramulu, D. Golberg, Y.-K. Han, D. P. Dubal, *Small* **2020**, *16*, 2002806.
[6] a) Y. Huang, M. Zhong, F. Shi, X. Liu, Z. Tang, Y. Wang, Y. Huang, H. Hou, X. Xie, C. Zhi, *Angew. Chem. Int. Ed.* **2017**, *56*, 9141–9145; b) K. Mishra, N. Devi, S. S. Siwal, Q. Zhang, W. F. Alsanie, F. Scarpa, V. K. Thakur, *Adv. Sci.* **2022**, *9*, 2202187.
[7] a) S. Karamveer, V. K. Thakur, S. S. Siwal, *Mater. Today: Proc.* **2022**, *56*, 9–17; b) H. Kaur, S. S. Siwal, G. Chauhan, A. K. Saini, A. Kumari, V. K. Thakur, *Chemosphere* **2022**, *304*, 135182; c) S. S. Siwal, A. K. Saini, S. Rarotra, Q. Zhang, V. K. Thakur, *J. Nanostruct. Chem.* **2021**; d) S. S. Siwal, Q. Zhang, N. Devi, K. V. Thakur, *Polymer* **2020**, *12*; e) S. S. Siwal, Q. Zhang, C. Sun, V. K. Thakur, *Nanomaterials* **2019**, *10*; f) M. Choudhary, S. Siwal, D. Nandi, K. Mallick, *Appl. Surf. Sci.* **2017**, *424*, 151–156.
[8] a) N. Devi, S. S. Siwal, *Nanofabrication* **2022**, *7*; b) S. S. Siwal, H. Kaur, G. Chauhan, V. K. Thakur, *Adv. NanoBiomed Res.* **2023**, *3*, 2200123; c) K.-B. Wang, Q. Xun, Q. Zhang, *EnergyChem* **2020**, *2*, 100025; d) X. Li, X. Yang, H. Xue, H. Pang, Q. Xu, *EnergyChem* **2020**, *2*, 100027.

[9] a) T.-H. Le, Y. Kim, H. Yoon, *Polymer* **2017**, *9*, 150; b) N. Devi, S. S. Ray, *Mater. Today Commun.* **2020**, *25*, 101691; c) N. Devi, S. K. Ghosh, V. K. Perla, K. Mallick, *ACS Omega* **2020**, *5*, 18693–18699; d) N. Devi, S. Ghosh, K. Mallick, *Inorg. Chem. Commun.* **2019**, *103*, 93–99; e) N. Devi, S. Ghosh, V. K. Perla, T. Pal, K. Mallick, *New J. Chem.* **2019**; f) N. Devi, S. Ghosh, S. C. Ray, K. Mallick, *ChemistrySelect* **2018**, *3*, 12057–12064.
[10] a) C. Chen, Z. Gan, C. Xu, L. Lu, Y. Liu, Y. Gao, *Electrochim. Acta* **2017**, *252*, 226–234; b) Z. Gan, N. Song, H. Zhang, Z. Ma, Y. Wang, C. Chen, *J. Electrochem. Soc.* **2020**, *167*, 085501; c) F. Liu, C. Wu, Y. Dong, C. Zhu, C. Chen, *J. Colloid Interface Sci.* **2022**, *628*, 682–690.
[11] A. I. Mtz-Enriquez, C. Gomez-Solis, A. I. Oliva, A. Zakhidov, P. M. Martinez, C. R. Garcia, A. Herrera-Ramirez, J. Oliva, *Mater. Chem. Phys.* **2020**, *244*, 122698.
[12] a) A. G. Olabi, Q. Abbas, M. A. Abdelkareem, A. H. Alami, M. Mirzaeian, E. T. Sayed, *Batteries* **2023**, *9*, 19; b) L. Vivas, D. P. Singh, *Front. Energy Res.* **2022**, *9*.
[13] a) Y.-R. Lv, Z.-L. Wang, Y.-X. Yang, Y. Luo, S.-Y. Yang, Y.-H. Xu, *J. Hazard. Mater.* **2022**, *432*, 128665; b) F. Zhao, H. Sheng, Q. Sun, J. Wang, Q. Liu, Z. Hu, B. He, Y. Wang, Z. L, X. Liu, *J. Colloid Interface Sci.* **2022**, *621*, 267–274; c) R. Manikandan, S. Sekar, S. P. Mani, S. Lee, D. Y. Kim, S. Saravanan, *Int. J. Hydrogen Energy* **2023**.
[14] M. I. A. Abdel Maksoud, N. M. Sami, H. S. Hassan, A. S. Awed, *Sep. Purif. Technol.* **2021**, *277*, 119478.
[15] A. Dittmer, J. Menze, B. Mei, J. Strunk, H. S. Luftman, R. Gutkowski, I. E. Wachs, W. Schuhmann, M. Muhler, *J. Phys. Chem. C* **2016**, *120*, 18191–18200.
[16] S. O. Alfaro, A. Martínez-de la Cruz, *Appl. Catal. A* **2010**, *383*, 128–133.
[17] S. Zeng, R. Tang, S. Duan, L. Li, C. Liu, X. Gu, S. Wang, D. Sun, *J. Colloid Interface Sci.* **2014**, *432*, 236–245.
[18] X. Y. Kong, T. Tong, B.-J. Ng, J. Low, T. H. Zeng, A. R. Mohamed, J. Yu, S.-P. Chai, *ACS Appl. Mater. Interfaces* **2020**, *12*, 26991–27000.
[19] M. Faisal, M. A. Rashed, J. Ahmed, M. Alsaiari, M. Jalalah, S. A. Alsareii, F. A. Harraz, *Chemosphere* **2022**, *287*, 131984.
[20] Y. Qiu, H. Fan, X. Chang, H. Dang, Q. Luo, Z. Cheng, *Appl. Surf. Sci.* **2018**, *434*, 16–20.
[21] N. M. Shinde, Q. X. Xia, J. M. Yun, S. Singh, R. S. Mane, K.-H. Kim, *Dalton Trans.* **2017**, *46*, 6601–6611.
[22] C. L. Vecchio, X. Lyu, I. Gatto, B. Zulevi, A. Serov, V. Baglio, C. L. Vecchio, I. Gatto, V. Baglio, *J. Power Sources* **2023**, *561*, 232732.
[23] A. Deepi, G. Srikesh, A. S. Nesaraj, *Nano-Struct. Nano-Objects* **2018**, *15*, 10–16.
[24] X. Zhai, J. Gao, X. Xu, W. Hong, H. Wang, F. Wu, Y. Liu, *J. Power Sources* **2018**, *396*, 648–658.
[25] L. Ma, Q. Zhao, Q. Zhang, M. Ding, J. Huang, X. Liu, Y. Liu, X. Wu, X. Xu, *RSC Adv.* **2014**, *4*, 41636–41641.
[26] M. Ciszewski, A. Mianowski, P. Szatkowski, G. Nawrat, J. Adamek, *Ionics* **2015**, *21*, 557–563.
[27] a) V. D. Nithya, R. Kalai Selvan, D. Kalpana, L. Vasylechko, C. Sanjeeviraja, *Electrochim. Acta* **2013**, *109*, 720–731; b) M. B. Tahir, T. Nawaz, G. Nabi, M. Sagir, M. Rafique, A. Ahmed, S. Muhammad, *Int. J. Hydrogen Energy* **2020**, *45*, 22833–22847; c) S. Zhong, C. Li, M. Shen, C. Lv, S. Zhang, *J. Mater. Res. Technol.* **2019**, *8*, 1849–1858; d) S. Gupta, R. Singh, M. D. Anoop, V. Kulshrestha, D. N. Srivastava, K. Ray, S. L. Kothari, K. Awasthi, M. Kumar, *Appl. Phys. A* **2018**, *124*, 737.
[28] a) A. Y. Arasi, J. J. L. Jeyakumari, B. Sundaresan, V. Dhanalakshmi, R. Anbarasan, *Spectrochim. Acta Part A* **2009**, *74*, 1229–1234; b) Y. Ding, J. Liang, G. Liu, W. Ni, L. Shen, *Coating* **2019**, *9*, 399.
[29] W. Zhang, L. Peng, J. Wang, C. Guo, S. H. Chan, L. Zhang, *Front. Chem.* **2020**, *8*.
[30] a) Q. Wu, Y. Xu, Z. Yao, A. Liu, G. Shi, *ACS Nano* **2010**, *4*, 1963–1970; b) X. Yu, J. Lu, C. Zhan, R. Lv, Q. Liang, Z.-H. Huang, W. Shen, F. Kang, *Electrochim. Acta* **2015**, *182*, 908–916.
[31] A. V. Radhamani, K. M. Shareef, M. S. R. Rao, *ACS Appl. Mater. Interfaces* **2016**, *8*, 30531–30542.
[32] a) P. Kumari, K. Khawas, S. Nandy, B. K. Kuila, *Electrochim. Acta* **2016**, *190*, 596–604; b) K. Zhang, L. L. Zhang, X. S. Zhao, J. Wu, *Chem. Mater.* **2010**, *22*, 1392–1401.

Manuscript received: May 12, 2023